Nano-encapsulation of Organic Phase Change Material in Water via Coacervation using Amphoteric Copolymer

Suqing Tan,[1] Albert P. C. Chan,[2] Pei Li*[1]

[1] Department of Applied Biology and Chemical Technology, The Hong Kong Polytechnic University, Hung Hom, Kowloon, Hong Kong, P. R. China

[2] Department of Building and Real Estate, The Hong Kong Polytechnic University, Hung Hom, Kowloon, Hong Kong, P. R. China

*Corresponding author: Email: pei.li@polyu.edu.hk

ABSTRACT: Nanoencapsulation of phase change materials is receiving increasing attention because of enhanced thermal conductivity and thermal capacity as well as ease of incorporation into the matrix for a wide range of applications. In this work, we have developed a simple and efficient approach to fabricating nanoencapsulated organic phase change (NEPCM) particles in water via coacervation using an amphoteric and temperature-sensitive copolymer. The chitosan-co-poly(methacrylic acid) (CTS-co-PMAA) copolymer plays dual functions as an emulsion stabilizer and a shell material. The fabrication involves emulsion formation, followed by

coacervation to form particle shell through adjusting solution pH, and finally rigidization of the shell via glutaraldehyde crosslinking. This method achieves high encapsulation efficiency (up to 94%) with a PCM content of 67%, high thermal capacity (LHs 165 J/g, and LHm 169 J/g), and high thermal cycling stability over 100 phase change cycles.

INTRODUCTION

Thermal energy storage (TES) systems based on phase change materials (PCM) are receiving increasing attention because of their ability to store and release latent heat during phase change with high energy storage capacity, high density, and narrow operating temperature.[1] In recent years, organic-based PCMs such as n-octadecane, n-hexadecane, n-nonadecane, n-docosane, fatty acids, fatty acid esters, as well as their binary and ternary mixtures are of particular interest due to their high thermal capacity (128-198 J/g), high thermal stability, low supercooling, ability to melt congruently, low chemical reactivity and low toxicity.[2] These features make them highly desirable in thermal energy storage for a wide range of applications.[3] However, organic PCMs suffer from low thermal conductivity.[4] The liquid-solid phase change poses technical difficulties when designing PCM-based TES systems.

Encapsulation of PCMs has been developed to address the above-mentioned problems.[5] They enable the PCM to be handled as either solid material or formulated into aqueous dispersion or powder, thus allowing for easy handling while preventing PCM from flowing away during its solid-liquid phase transition. Encasing PCM with a shell also serves to protect the PCM from the external environment, e.g. contamination, chemical reaction, and prevention of vaporization. Other advantages also include increased heat transfer area due to the increased surface-to-volume ratio,

reduced volume change during phase transition, enhanced mechanical stability in heating-cooling cycles, and reduced PCM toxicity.[1, 6]

Traditional organic PCM encapsulation methods involve spray drying,[7-8] suspension polymerization,[9] interfacial polymerization,[10-13] emulsion polymerization,[14-16] in-situ polymerization,[17] sol-gel method[18-21], coacervation[22-24] or phase separation[25], etc. These approaches usually produce capsules with diameters in the micron-scale range. Nanoencapsulation of PCM (NEPCM) has received increasing attention because of its further advantages: 1) their smaller size denotes a relatively larger surface area for heat transfer; 2) the NEPCM reduces complications such as pipe abrasion and clogging, thus allowing them to be used for thermal fluids with enhanced thermal conductivity[26] and thermal capacity[27]; 3) The NEPCM can be easily incorporated into a various matrix for a wide range of application.

Currently, the main approaches to preparing NEPCM include emulsion polymerization[28-30]; miniemulsion polymerization[31-34]; *in situ* polymerization[35-37] and sol-gel method[38-40]. These polymerization methods often have complications of residual monomer while the sol-gel process is both time-consuming and uses relatively costly metal alkoxides. Furthermore, except for polymerizable emulsifiers,[34] additional surfactants are required to disperse and stabilize the nano-sized PCM droplets before encapsulation. The presence of surfactant may affect the thermal and mechanical properties of the NEPCMs. Although coacervation methods to produce microencapsulated PCMs have been extensively developed through the interaction of two polymers with opposite charges, this approach has only been scarcely studied in the synthesis of nano-encapsulated organic PCM.[41]

In this study, we present a coacervation method that is capable of producing nano-sized PCM encapsulates using a novel type of amphoteric and temperature-sensitive copolymer as shell

material without the addition of emulsifiers. The polymer plays dual functions as stabilizer and shell material with tunable surface-active properties at different pH and temperature. The fabrication involves emulsion formation, followed by coacervation through adjusting solution pH, and finally rigidization of the shell via glutaraldehyde crosslinking. All of these steps were carried out under mild reaction conditions. This method achieves high encapsulation efficiency (up to 94%) with a PCM content of 67%, high thermal capacity (LHs 165 J/g, and LHm 169 J/g), and high thermal cycling stability over 100 phase change cycles.

MATERIALS AND METHODS

Materials

Methacrylic acid (MAA) monomer (Sigma-Aldrich) was purified via passing through a column prepacked with inhibitor remover (Sigma-Aldrich). Chitosan (CTS) was obtained from AKBIO. Its degree of deacetylation (DAA) determined by elemental analysis was 72.5%. Hexadecane (C16), eicosane, acetic acid, *tert*-butyl hydroperoxide (TBHP), KOH and glutaraldehyde (GAL, 50 wt%) were all obtained from Sigma-Aldrich and used as received. Hexane (99%) was purchased from Merck. Deionized water (Milli-Q purified) was used as the dispersion medium.

Synthesis of chitosan-co-poly(methacrylic acid)

For a total volume of 100 mL, chitosan (1.0 g) was first dissolved in 0.6% acetic acid solution by stirring for 2 h at 60℃ in a water-jacketed reactor. Purified MAA (1 g) was then added to the CTS solution and stirred at 500 rpm at 80℃ under atmospheric conditions for 24 h. The mixture was then purged with nitrogen for 30 min, followed by the addition of 1 mL (100 mM

TBHP) to initiate the polymerization. The reaction was further carried out at 80℃ for 2 h. Monomer conversion was close to 100%, and the resulting polymer solution was used for subsequent PCM encapsulation.

Synthesis of nano-encapsulated PCM

Eicosane (Ei) and hexadecane (C16) with a weight ratio of 1:10 were heated at 60℃ for 30 min with gentle swirling. The above prepared CTS-co-PMAA polymer solution (pH 1.4-1.7, 2 wt%, 9 mL) was also heated to 60℃. The Ei+C16 mixture (1 mL) was added to the polymer solution followed by sonication (SONICS VC130) at 5 W for 30 min. The emulsion was then placed in a refrigerator at 4℃ for 1 h. After which the emulsion was gently stirred while pH was increased to up to 7 by addition of 0.1M KOH at a rate of 1 drop/4 sec using a dropping funnel. GAL (0.492 g of 50 wt%) was diluted in 10 mL of water and added drop by drop (1 drop/4 sec) with gentle stirring. Stirring was continued for 1 h followed by increasing pH to up to 10 by addition of 0.1M KOH at a rate of 1 drop/4 sec. The reaction mixture was continuously stirred for 24 h at room temperature. After the reaction, un-encapsulated or partially encapsulated PCM were removed by hexane extraction. Approximately 50 mL of hexane was added to 150-200 mL of unpurified NEPCM mixture in a separating funnel. The bottom aqueous product was removed and then centrifuged twice (12 k rpm for 30 min) to remove excess CTS-co-PMAA and unreacted GAL. The lower density of the NEPCMs formed a pellet on top of the supernatant. The coacervates were then washed with 0.01 M KOH solution.

Measurement and characterization

Samples of CTS, MAA modified CTS intermediate and CTS-co-PMAA were all identified with a Bruker 400 MHz spectrometer. The samples were dried in an oven to remove water and any unreacted monomer followed by re-dissolution in a 2 wt% d-acetic acid in D_2O with sonication. All ^{1}H-NMR spectra were referenced internally to the residual proton resonance D_2O (4.79 ppm). The chemical structures of CTS-co-PMAA and NEPCM were identified with an FT-IR (Nicolet iS50 FT-IR) in the range between 4000 and 500 cm^{-1} using the attenuated total reflectance (ATR) method. The samples were dried for 2 days to remove moisture or ethanol before FT-IR measurement.

Particle size and size distribution of the CTS-co-PMAA and NEPCMs were measured with the Dynamic Light Scattering (DLS). The DLS measurement was performed with a Zetasizer Nano (Malvern) using a photon correlation spectroscopy with electrophoretic dynamic light scattering (a two-laser diode light source with a wavelength of 632.8 nm at 4 mW) operating at a detector angle of 173°. Samples were diluted to 500 ppm with either 0.1 M HCl (pH ~1.5) for CTS-co-PMAA or 0.01 M KOH for NCPCMs. Results of particle size (Z_{AVE}) were an average of triplicate measurements. For *zeta*-potential measurements, samples were diluted to 500 ppm in 1 mM NaCl and measured at room temperature with a Delsa Nano C Particle Analyzer (Beckman Coulter, Brea, CA, USA) coupled with the auto-titrator accessory. The *zeta*-potential measurements were measured with a monochromatic laser beam at 658 nm. Samples were freeze-dried, re-dispersed in either 0.1 M HCl or 0.1 M NaOH. For *zeta*- potential across a pH range, an auto-titrator accessory was used to adjust the pHs of the samples from pH 1.5 to 7 and pH 10 to 7 with solutions of 0.1 M NaOH and 0.1 M HCl, respectively.

For SEM imaging, 10 µL of the sample (100 ppm) onto a 3 mm diameter glass slide was either air-dried at room temperature and then placed in a desiccator or freeze-dried to remove moisture, followed by gold sputtering. SEM images were taken on a JEOL SM-31010 with an accelerating voltage of 5 kV.

The thermal stability of NEPCMs was studied with thermogravimetric analysis (TGA/DSC+ Mettler Toledo). A known amount of sample (1- 5 mg) was placed in an aluminum oxide sample holder. The sample was heated under a nitrogen atmosphere with a flow rate of 20 mL/min. The heating profile used was 60-600℃ (ramp: 10℃/min). TGA graphs were plotted using Origin. The weight was normalized and the first derivative was calculated with Saviztky-Golay smooth with a polynomial order of 2 and points of the window as 20.

Thermal properties of the NEPCMs were obtained with a differential scanning calorimetry (DSC) (Mettler Toledo, 822e). The temperature profile used in the DSC scan was a freezing profile from 25 to -10 °C, followed by a heating profile from -10 to 25 °C at a rate of 4 °C min^{-1}. The sample was first scanned at a rate of 10 °C min^{-1} to ensure unencapsulated PCM droplets (if present) had destabilized. During the DSC scan, nitrogen was passed through the sample chamber at 20 mL/min for protection. The encapsulation efficiency (%ee) is calculated according to Equations 1 and 2.

$$\%\mathbf{PCM} = \frac{\mathbf{LH_{s\ (NEPCM)}}}{\mathbf{249.14}} \times \mathbf{100}\% \qquad \text{Equation 1}$$

$$\%\mathbf{ee} = \frac{\mathbf{\%PCM \times Total\ Weight\ of\ NEPCM}}{\mathbf{Initial\ PCM\ added}} \qquad \text{Equation 2}$$

Where $LH_{s\ (NEPCM)}$ is the enthalpy of solidification (J/g) for the NEPCMs which is divided by the enthalpy of solidification of the PCM encapsulated, hexadecane (249.14 J/g). The NEPCMs were

cycled from 25 to -10 °C to -10 to 25 °C repeatedly at a rate of 20°C min^{-1} over 100 phase change cycles. The %ee before and after phase change cycling was compared to assess the loss of thermal capacity or PCM leakage.

RESULTS AND DISCUSSION

Synthesis and characterization of chitosan-co-poly(methacrylic acid)

Figure 1 shows the synthetic route to the amphoteric copolymer, CTS-co-PMAA. The chitosan was first modified with the methacrylic acid through an amidation reaction between the amine group of the chitosan and carboxylic acid group of MAA to form the intermediate product, MAA modified CTS containing double bond (A). This was followed by polymerization initiated via a redox reaction between TBHP and amine groups on the chitosan backbone to generate free radicals on the amine nitrogen atoms according to our previously established method.[43] The resultant radicals enabled graft polymerization of MAA monomer. At the same time, crosslinking reaction might occur, giving a transparent yellow solution upon acid addition. Various MAA to CTS weight ratios (1:2, 1:1 and 2:1) were synthesized according to the same procedure, and all of which yielded monomer conversion close to 100%. Subsequent results of encapsulation studies suggested that MAA to CTS = 1:1 weight ratio was the most optimal. Therefore, the weight ratio of MAA to CTS = 1:1 was used in further studies. Morphology of the CTS-co-PMAA polymer was observed with SEM image, showing fiber-like structure (Figure S1, Supporting Information).

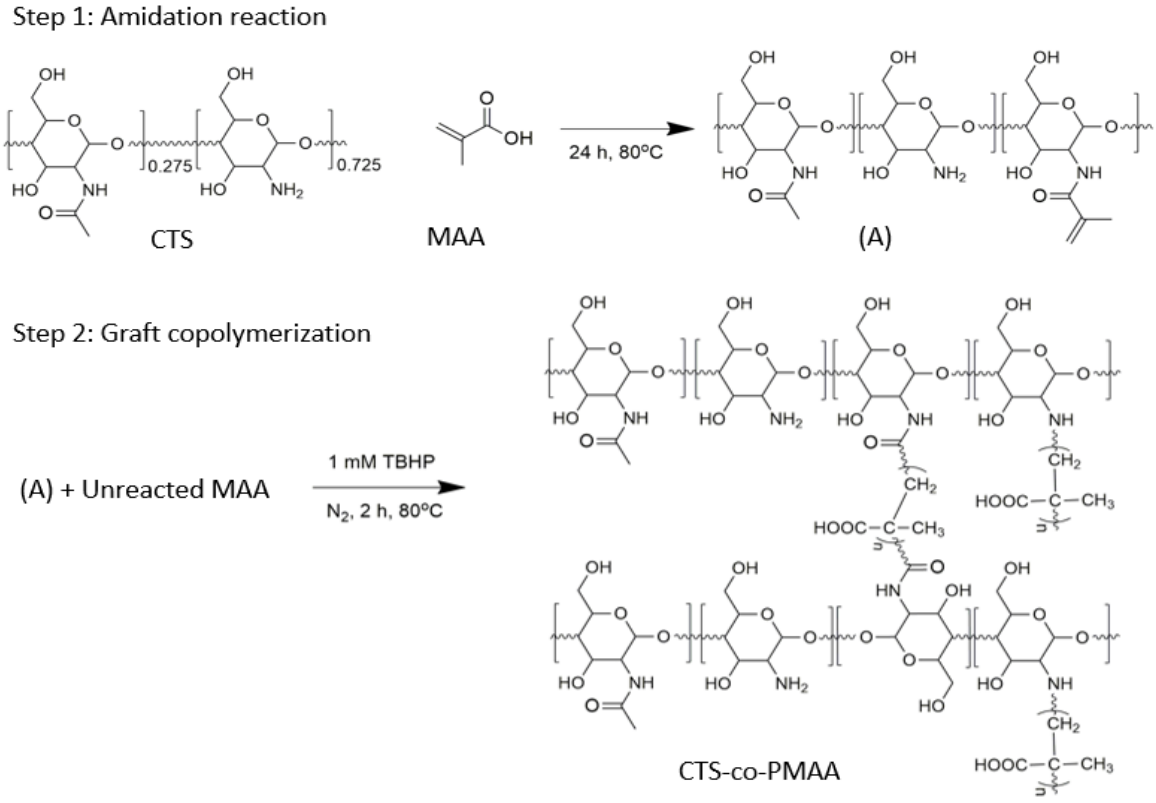

Figure 1. Proposed two-step reaction mechanism for the synthesis of CTS-co-PMAA

Figure 2 shows ^{1}H-NMR spectra of MAA monomer, MAA-modified chitosan (A) and chitosan-co-PMAA. Compared with the spectrum of MAA monomer, the modified chitosan possesses vinylic protons as observed at chemical shifts of 5.9 and 5.5 ppm. The H_d peak slightly shifted upfield from 6.0 (H1) to 5.9 pm, suggesting an amidation reaction between chitosan and the MAA. Furthermore, protons of methyl groups from both chitosan and MAA were found at 1.9 (H_g) and 1.8 (H_f) ppm, respectively. The relative ratio of the vinylic and methyl proton peaks gave almost the same value as of the original MAA, indicating that the major reaction was the amidation reaction. Calculations based on integral ratio indicated that the graft yield of MAA on to CTS was

11 wt% which agrees with monomer conversation determination based on the gravimetric method. Figure 2 also shows the ^{1}H-NMR spectrum of CTS-co-PMAA. Both vinylic hydrogens and the H_f protons of MAA disappeared, and a new and broad peak appeared between 0.7 and 1.5 ppm, signifying successful polymerization of MAA.

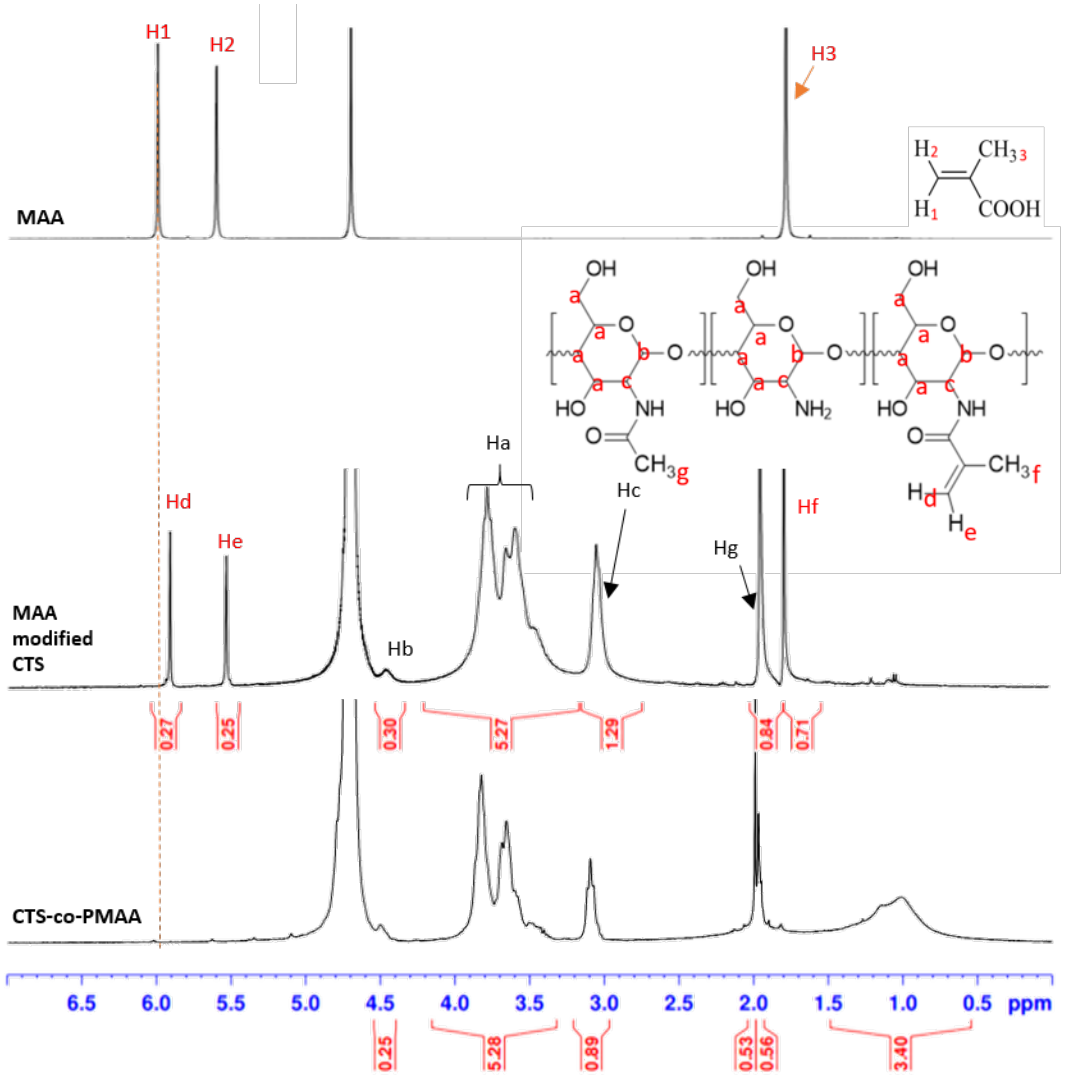

Figure 2. ^{1}H-NMR spectra of MAA monomer, MAA modified CTS and CTS-co-PMAA (All samples were dissolved in 2 wt% d-acetic acid in D_2O. The D_2O solvent peak is at 4.8 ppm).

Figure 3 shows FTIR spectra of CTS, MAA modified CTS, and CTS-co-PMAA. The chitosan with a degree of deacetylation of 72.5% displayed several characteristic bands. It has a broad peak of O-H and N-H stretching at 3256 cm^{-1}, amide stretching at 1632 cm^{-1}, N-H bending from amine at 1552 cm^{-1}, $-CH_2$ bending (1464 cm^{-1}), $-CH_3$ symmetrical deformation at 1413 cm^{-1} as well as C-O stretching at 1069 and 1020 cm^{-1}). After modification of CTS with MAA, the spectrum of the MAA modified CTS shows C=C and amide stretching at 1648 cm^{-1} with increased peak intensity, and C-N stretching band at 1065 cm^{-1}. The spectrum of the CTS-co-PMAA shows typical peaks of the carboxylic acid group (a very broad O-H stretching band in the 3600 -2500 cm^{-1} region, C=O stretching at about 1698 cm^{-1}, C-O stretching at 1152 cm^{-1}) Other characteristic bands of CTS are also identified. These FTIR results confirmed the chemical structures of the CTS-co-PMAA and its formation mechanism.

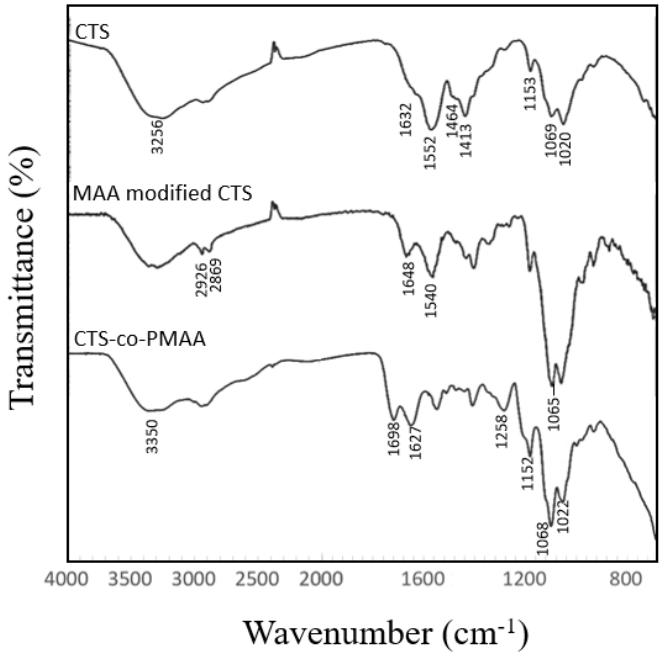

Figure 3. FTIR spectra of chitosan, MAA modified chitosan and CTS-co-PMAA synthesized with chitosan to MAA weight ratio of 1:1.

The chitosan-co-poly(methacrylic acid) is an amphoteric copolymer that is highly sensitive to the solution pH. In an acidic solution at a pH below 4.8,[44] the carboxylic acid group of the PMAA is protonated (pK_a of the carboxylic acid group is 4.8), while at neutral pH is almost deprotonated. On the other hand, since the pK_a of the primary amine group of the chitosan is 6.5,[18] the chitosan is highly soluble at low solution pH, but it becomes insoluble above pH of 6.5. Therefore, the solubility of CTS-co-PMAA could be manipulated by turning the solution pH across the pH range. The pH sensitivity of the CTS-co-PMAA is demonstrated through the *zeta*-potential measurement as a function of pH (Figure 4). At pH 2.5, the polymer has a positive surface charge of around +38 mV. It decreases rapidly at pH 4 which coincides with the pKa value of the PMAA moiety. The isoelectric point of the resultant polymer was around pH 5.6. Upon further pH increase, the protonated amine group loses its charge ($NH^{3+} \rightarrow NH_2$, *p*Ka 6.5) and the surface charge of CTS-co-PMAA becomes increasingly negative until it reaches a maximum negative surface charge around -35 mV after pH 8.

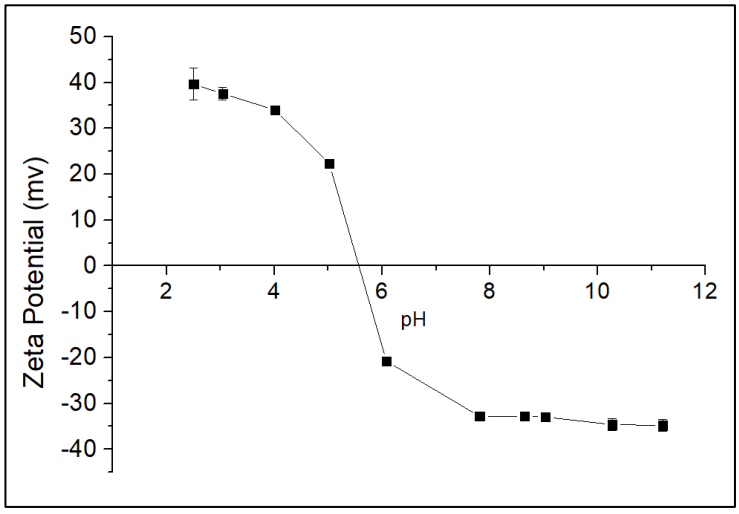

Figure 4. *zeta*-Potential curve of CTS-co-PMAA (1:1 weight ratio) as a function of pH in 1 mM of NaCl.

Synthesis and characterization of NEPCMs with CTS-co-PMAA

The NEPCMs were synthesized using hexadecane (C16) as PCM core, 10 wt% eicosane as a nucleating agent, and CTS-co-PMAA as a shell material. Scheme 1 illustrates the fabrication procedure: 1) Emulsion formation where the core material is dispersed in the polymer solution; 2) Coacervation through depositing the copolymer onto the PCM droplets via adjusting solution pH from 1.5 to 5.6; 3) Rigidization of the shell via glutaraldehyde crosslinking.

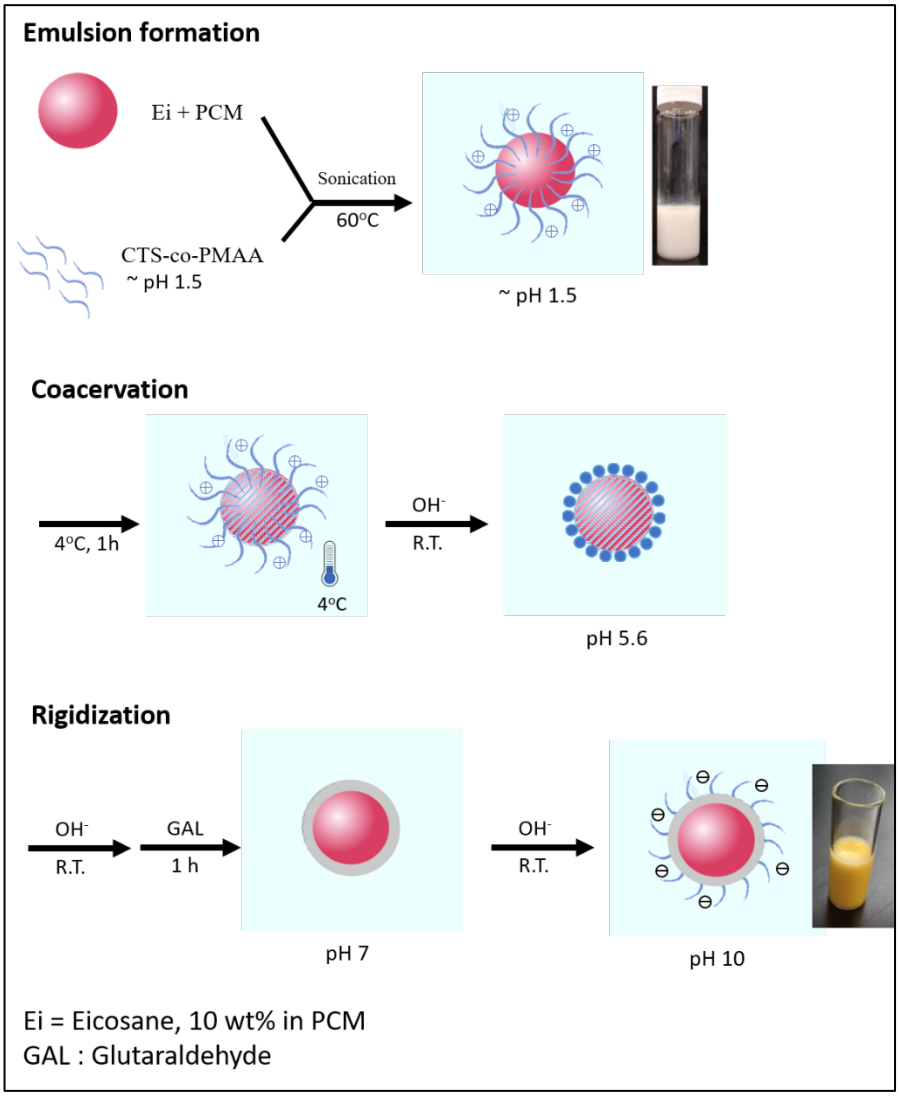

Scheme 1. Schematic diagram of NEPCM synthesis

Stable emulsion could not form when simply mixing or homogenizing the PCM in a CTS-co-PMAA solution. However, when dispersing the PCM in CTS-co-PMAA solution under a high-powered sonication process (5 W, 30 min with SONICS VC130), a stable emulsion was formed which showed no phase separation after several months. To understand this effect, we have investigated the solubility of the CTS-co-PMAA as a function of temperature. It was found that its solubility decreased with increasing solution temperature as illustrated in Figure S2 (Supporting Information). Turbidity measurement indicated that the phase transition took place around 73 ºC (Figure S3, Supporting Information), which may be due to the weakening of the hydrogen bonds between CTS-co-PMAA and water at high temperatures, thus increasing intra- or inter-polymer hydrogen bonding between carboxylic acid groups from PMAA and hydroxyl groups of the chitosan. On the other hand, simply raising the solution temperature with agitation is insufficient to form stable emulsions. Therefore, we propose that because the CTS-co-PMAA possesses temperature-induced surface-active property, it enables micelle formation during sonication, resulting in encapsulation of the PCM into the particles through their hydrophobic interaction.

After forming the CTS-co-PMAA stabilized C16 emulsions, coacervation of the CTS-co-PMAA began by placing the emulsion in a refrigerator (~ 4 °C, 1 h) to solidify the PCM. This step serves to prevent the coalescence of the particles in the ensuing base titration which result in the formation of nano-sized encapsulates. Base titration caused precipitation of the polymer via the formation of NH^{3+}/COO^{-} complexes, leading to coarsening of the emulsion around pH 5.6-5.8 which coincides with the isoelectric point previously measured. Upon further increase of the pH ($NH^{3+} \rightarrow NH_2$, pKa 6.5), the coarsened emulsion was no longer observed, and the particles were stabilized via negatively charged COO^{-} groups from the PMAA moiety.

After forming the CTS-co-PMAA encapsulated PCM particles, rigidization of the shell was carried out by adding the chemical crosslinker, glutaraldehyde at pH 7, followed by further titration to pH 10 to completely precipitate the CTS moiety of the particle to increase the rigidity. The high pH is selected as a precaution as previous studies indicated the encapsulates (before GAL crosslinking) at pH 7 to have zeta potential ~9.2 mV which is insufficient to form stable dispersions. The resulting particles were finally washed with hexane to remove unencapsulated PCM. The NEPCM was then collected by centrifugation. Figure S4 (Supporting Information) shows its appearance in water dispersion and dried powder form. Their light yellow color was due to GAL crosslinking.[45] The synthesized NEPCMs were sufficiently rigid to withstand water removal under conditions such as drying and ultrafiltration. DSC results indicated retention of up to 60% of the PCM upon freeze-drying (Figure S5 Supporting Information). The resultant NEPCMs had a surface charge of -50.4±7.9 mV at pH 10 and showed no signs of precipitation or phase separation over several months.

Properties of NEPCM particles

FTIR spectra of the hexadecane, CTS-co-PMAA, and NEPCM are shown in Figure 5. The imine bond (C=N) is identified at 1548 cm^{-1} for the NEPCM, suggesting the formation of Schiff base during glutaraldehyde crosslinking with the amine of chitosan. A broad peak at 1647 cm^{-1} indicates the presence of carboxylic acid and amide groups. Characteristic peaks of hexadecane between 2956 and 2872 cm^{-1} as well as 1466 cm^{-1} are also identified in the NEPCM sample. These results indicate successful encapsulation of the PCM and retention of the PCM after drying.

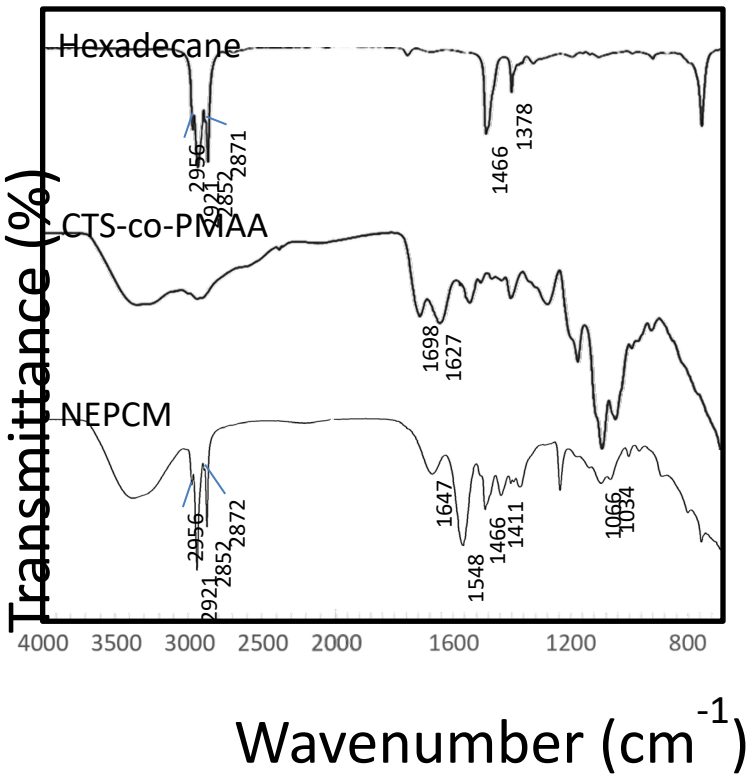

Figure 5. FTIR spectra of hexadecane, CTS-co-PMAA and NEPCM

Thermal stability of the NEPCM

The decomposition behavior of the NEPCMs was determined with thermogravimetry (Figure 6). The TGA curve indicates that the decomposition occurs in five mass loss steps. The endothermal DTG peaks are directly related to the occurring mass loss steps: 1) Release of water below 100 °C (4%); 2) Evaporation of hexadecane and eicosane at temperatures ranging from 142 – 228 °C (20%)[46-47]; 3) Mass loss of polymer shell occurred between 228 and 340 °C (32%); 4) and 5) After the decomposition of the shell material, the encapsulated hexadecane and eicosane evaporated as exhibited by two sharp peaks at 338 °C and 344 °C, respectively (44%). The mass ratio of PCMs (hexadecane + eicosane) to shell material is approximately 66.7/33.3. These results

also suggest that the shell material is capable of preventing at least part of the encapsulated PCM from evaporation.

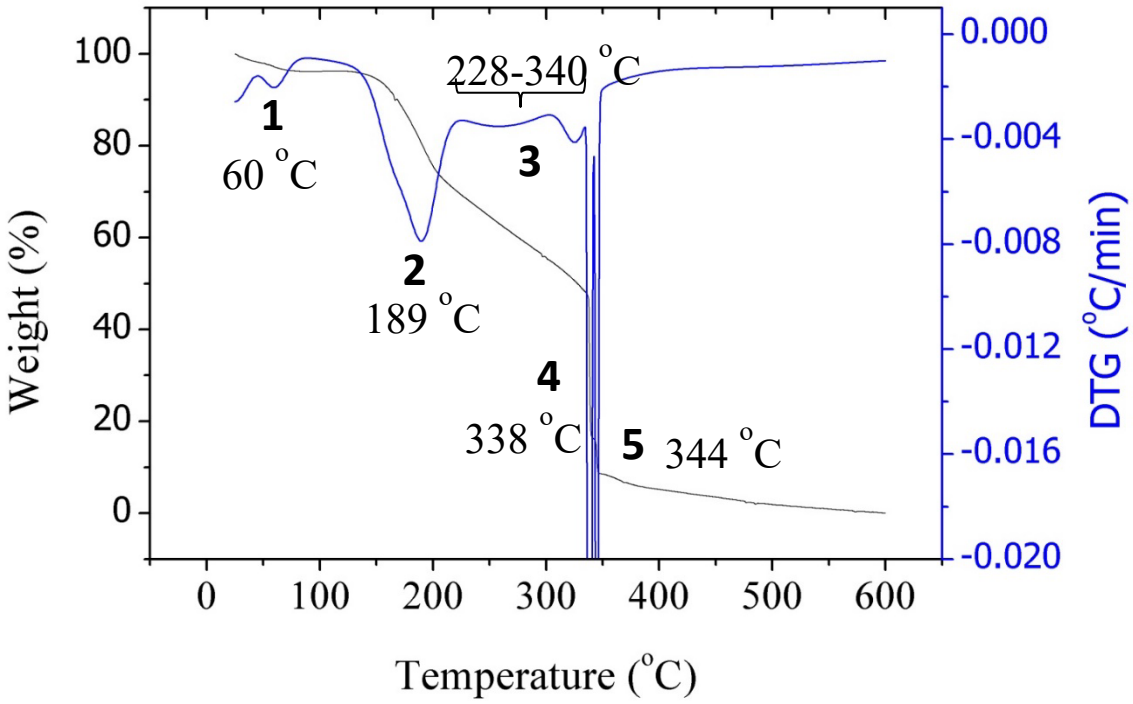

Figure 6. Thermogravimetric analysis of the NEPCMs

Particle size and morphology of the NEPCM particles

Figure S6 (Supporting Information) shows that the average hydrodynamic diameter of the NEPCMs was 438 nm with a polydispersity of 0.22. Figure 7 displays SEM images of the dried NEPCMs. They are spherical particles with an average diameter of 243 ± 69 nm, which is approximately half the hydrodynamic diameter. This size shrinkage is due to the collapse of the extended PMAA moiety located on the NEPCM shell upon removal of water.

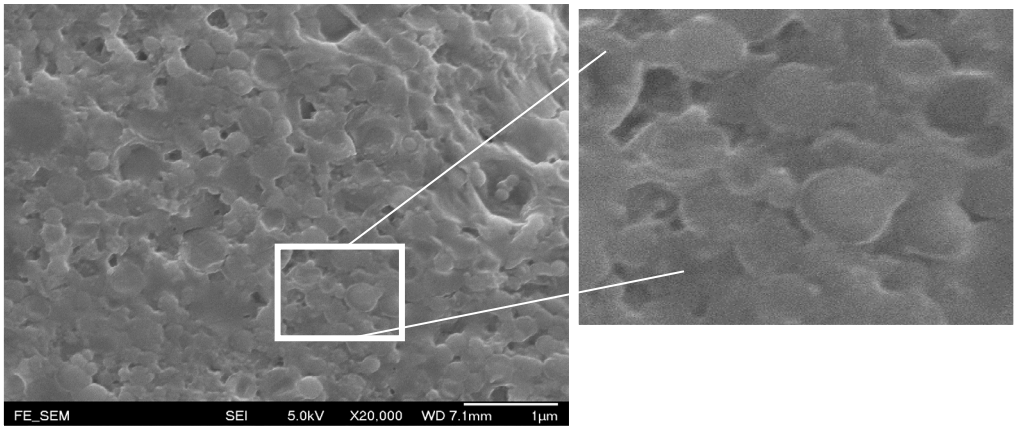

Figure 7. SEM images of NEPCM (estimated average diameter is 243 ± 69 nm)

Phase change property of the NEPCM

Figure 8 shows the thermal profiles of the NEPCMs up to 100 phase change cycles. It possessed a thermal capacity of LH_s 165 J/g and LH_m 169 J/g. The PCM content was 67 wt%. based on the calculation using Equation 1. For thermal energy storage applications, the NEPCMs were also assessed for their stability of freeze-thaw cycling using DSC. The thermal profiles of the NEPCMs at 0, 20, and 100 cycles are denoted as HF0, HF20, and HF100, respectively. Enthalpy values of NEPCMs after 20 and 100 cycles were LH_s 165 J/g, LH_m 169 J/g, and LH_s 165 J/g, LH_m 163 J/g, respectively. There is negligible change in the area and structure of the exothermic and the endothermic peaks, signifying high cycling stability of the NEPCMs after 100 phase change cycles"

However, the NEPCMs exhibited supercooling, which is the depression of the PCM's freezing temperature. This phenomenon is due to the nano-confinement effect of the PCM, which markedly increases as the dimensions of the NEPCMs decrease.[48] Although adding a nucleating agent, eicosane, showed reduced supercooling, the supercooling still could not be completely

eliminated even with the addition of up to 10 wt% eicosanes in hexadecane. The NEPCMs also possessed a broad exothermic peak with multiple peaks from 9 to -7.9 ℃ and a broad endothermic peak at 8.4-19.5 ℃. The broad phase transition temperatures may be attributed to the presence of nucleating agents and variation of the NEPCM particle size.

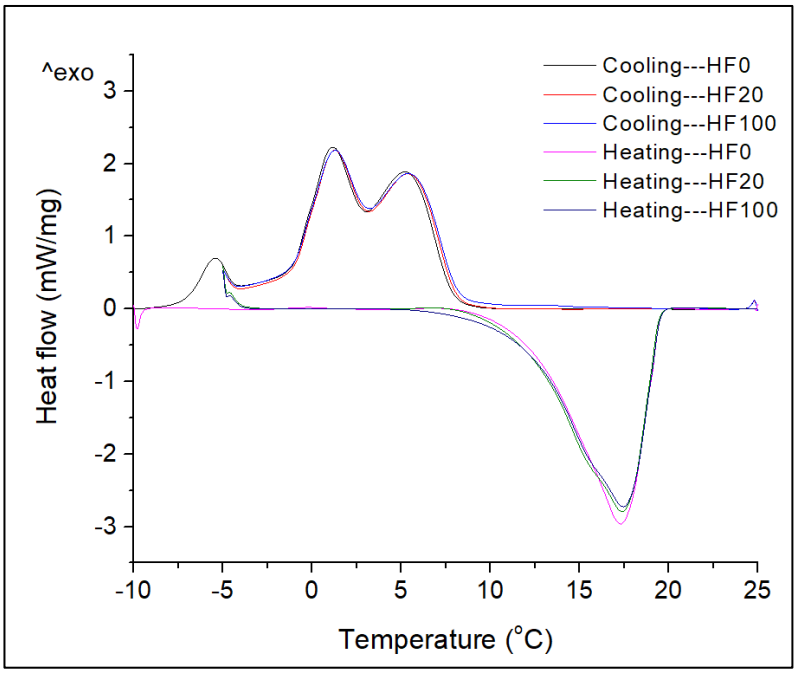

Figure 8. DSC curves and thermal characteristics of the NEPCMs over 100 phase change cycles

CONCLUSION

A novel type of amphoteric and temperature-sensitive copolymer, chitosan-co-poly(methacrylic acid) has been synthesized and carefully characterized for its chemical structures, pH, and temperature-induced surface-active property. The CTS-co-PMAA copolymer was able to play a dual role: as an emulsion stabilizer and a shell material for preparing nano-encapsulated PCM through first emulsion formation, followed by coacervation through adjusting solution pH,

and finally rigidization of the shell via glutaraldehyde crosslinking. The NEPCMs possess the following features: 1) Nanoencapsulated PCM particles ranging from 140 to 310 nm in diameter and were highly stable in the aqueous system without the need to use surfactant for stabilization. 2) High encapsulation efficiency up to 94% with a PCM content of 67% and high thermal capacity (LH_s 165 J/g, and LH_m 169 J/g). 3) High shell integrity, resistance to solvent extraction, freeze-dry, and volatilization. 4) Withstand up to 100 phase change cycles without discernible change in exothermic and endothermic peaks after 100 phase change cycles, signifying high thermal cycling stability. ~~5) Antibacterial property due to the presence of chitosan.~~ On the other hand, the nano-encapsulation PCM lead to broader phase transition temperature with the supercooling issue.

ASSOCIATED CONTENT

Supporting Information

The Supporting Information is available free of charge on the ACS Publications website at DOI: Morphology of the CTS-co-PMAA polymer observed with SEM image; Turbidity of CTS-co-PMAA vs temperature; Appearance of NEPCM dispersion in water and dried powder; TGA curve of chitosan and CTS-co-PMAA (1:1); Particle size and size distribution of CTS-co-PMMA encapsulated hexadecane particles

AUTHOR INFORMATION

Corresponding Author: *Email:pei.li@polyu.edu.hk

ORCID: Pei Li: 0000-0001-9098-7598

Notes: The authors declare no competing financial interest.

Funding Sources:

Research Institute of Sustainable Urban Development (RISUD) and The Hong Kong Polytechnic University

ACKNOWLEDGEMENT

We gratefully acknowledge the financial support from the Research Institute of Sustainable Urban Development, The Hong Kong Polytechnic University (Project code RTPB).

REFERENCES

1. Dincer, I.; Rosen, M., *Thermal energy storage: systems and applications*. John Wiley & Sons: 2002.
2. Tyagi, V. V.; Kaushik, S. C.; Tyagi, S. K.; Akiyama, T., Development of phase change materials based microencapsulated technology for buildings: a review. *Renewable and Sustainable Energy Reviews* **2011,** *15* (2), 1373-1391.
3. Sharma, R. K.; Ganesan, P.; Tyagi, V. V.; Metselaar, H. S. C.; Sandaran, S. C., Developments in organic solid-liquid phase change materials and their applications in thermal energy storage. *Energy Conversion and Management* **2015,** *95*, 193-228.
4. Himran, S.; Suwono, A.; Mansoori, G. A., Characterization of alkanes and paraffin waxes for application as phase change energy storage medium. *Energy Sources* **1994,** *16* (1), 117-28.
5. Alva, G.; Lin, Y.; Liu, L.; Fang, G., Synthesis, characterization and applications of microencapsulated phase change materials in thermal energy storage: A review. *Energy and Buildings* **2017,** *144*, 276-294.
6. Zhao, C. Y.; Zhang, G. H., Review on microencapsulated phase change materials (MEPCMs): Fabrication, characterization and applications. *Renewable and Sustainable Energy Reviews 15* (8), 3813-3832.
7. Borreguero, A. M.; Valverde, J. L.; RodrÃguez, J. F.; Barber, A. H.; Cubillo, J. J.; Carmona, M., Synthesis and characterization of microcapsules containing Rubitherm®RT27 obtained by spray drying. *Chemical Engineering Journal 166* (1), 384-390.
8. Rosenberg, M.; Kopelman, I. J.; Talmon, Y., Factors affecting retention in spray-drying microencapsulation of volatile materials. *Journal of Agricultural and Food Chemistry* **1990,** *38* (5), 1288-1294.

9. Hawlader, M. N. A.; Uddin, M. S.; Khin, M. M., Microencapsulated PCM thermal-energy storage system. *Applied Energy* **2003,** *74* (1), 195-202.
10. Suzuki, T.; Mizowaki, T.; Okubo, M., Versatile synthesis of high performance, crosslinked polymer microcapsules with encapsulated n-hexadecane as heat storage materials by utilizing microsuspension controlled/living radical polymerization (ms CLRP) of ethylene glycol dimethacrylate with the SaPSeP method. *Polymer* **2016,** *106* (Supplement C), 182-188.
11. Cho, J.-S.; Kwon, A.; Cho, C.-G., Microencapsulation of octadecane as a phase-change material by interfacial polymerization in an emulsion system. *Colloid Polym. Sci.* **2002,** *280* (3), 260-266.
12. Wei, J.; Li, Z.; Liu, L.; Liu, X., Preparation and characterization of novel polyamide paraffin MEPCM by interfacial polymerization technique. *Journal of Applied Polymer Science* **2013,** *127* (6), 4588-4593.
13. Lone, S.; Lee, H. M.; Kim, G. M.; Koh, W.-G.; Cheong, I. W., Facile and highly efficient microencapsulation of a phase change material using tubular microfluidics. *Colloids and Surfaces A: Physicochemical and Engineering Aspects* **2013,** *422*, 61-67.
14. Alkan, C.; Sari, A.; Karaipekli, A., Preparation, thermal properties and thermal reliability of microencapsulated n-eicosane as novel phase change material for thermal energy storage. *Energy Convers. Manage.* **2010,** *52* (1), 687-692.
15. Alay, S.; Göde, F.; Alkan, C., Synthesis and thermal properties of poly(n-butyl acrylate)/n-hexadecane microcapsules using different cross-linkers and their application to textile fabrics. *Journal of Applied Polymer Science* **2011,** *120* (5), 2821-2829.
16. Ma, S.; Song, G.; Li, W.; Fan, P.; Tang, G., UV irradiation-initiated MMA polymerization to prepare microcapsules containing phase change paraffin. *Solar Energy Materials and Solar Cells* **2010,** *94* (10), 1643-1647.
17. Yin, D.; Ma, L.; Liu, J.; Zhang, Q., Pickering emulsion: A novel template for microencapsulated phase change materials with polymerâ€“silica hybrid shell. *Energy 64* (0), 575-581.
18. Zhang, H.; Wang, X.; Wu, D., Silica encapsulation of n-octadecane via sol–gel process: A novel microencapsulated phase-change material with enhanced thermal conductivity and performance. *Journal of Colloid and Interface Science* **2010,** *343* (1), 246-255.
19. He, F.; Wang, X.; Wu, D., New approach for sol–gel synthesis of microencapsulated n-octadecane phase change material with silica wall using sodium silicate precursor. *Energy* **2014,** *67*, 223-233.
20. Li, M.; Wu, Z.; Tan, J., Properties of form-stable paraffin/silicon dioxide/expanded graphite phase change composites prepared by sol–gel method. *Applied Energy* **2012,** *92*, 456-461.
21. Chen, Z.; Cao, L.; Shan, F.; Fang, G., Preparation and characteristics of microencapsulated stearic acid as composite thermal energy storage material in buildings. *Energy and Buildings* **2013,** *62*, 469-474.
22. Konuklu, Y.; Unal, M.; Paksoy, H. O., Microencapsulation of caprylic acid with different wall materials as phase change material for thermal energy storage. *Solar Energy Materials and Solar Cells* **2014,** *120*, 536-542.
23. Hawlader, M. N. A.; Uddin, M. S.; Khin, M. M., Microencapsulated PCM thermal-energy storage system. *Appl. Energy* **2003,** *74* (1-2), 195-202.

24. Özonur, Y.; Mazman, M.; Paksoy, H. Ö.; Evliya, H., Microencapsulation of coco fatty acid mixture for thermal energy storage with phase change material. *International Journal of Energy Research* **2006,** *30* (10), 741-749.
25. Yang, R.; Zhang, Y.; Wang, X.; Zhang, Y.; Zhang, Q., Preparation of n-tetradecane-containing microcapsules with different shell materials by phase separation method. *Solar Energy Materials and Solar Cells* **2009,** *93* (10), 1817-1822.
26. Harikrishnan, S.; Devaraju, A.; Kumar, G. R.; Kalaiselvam, S., Improved thermal energy storage behavior of a novel nanofluid as phase change material (PCM). *Materials Today: Proceedings* **2019,** *9*, 410-421.
27. Buttitta, G.; Serale, G.; Cascone, Y., Enthalpy-temperature Evaluation of Slurry Phase Change Materials with T-history Method. *Energy Procedia* **2015,** *78*, 1877-1882.
28. Tumirah, K.; Hussein, M. Z.; Zulkarnain, Z.; Rafeadah, R., Nano-encapsulated organic phase change material based on copolymer nanocomposites for thermal energy storage. *Energy (Oxford, U. K.)* **2014,** *66*, 881-890.
29. Chen, C.; Chen, Z.; Zeng, X.; Fang, X.; Zhang, Z., Fabrication and characterization of nanocapsules containing n-dodecanol by miniemulsion polymerization using interfacial redox initiation. *Colloid Polym. Sci.* **2012,** *290* (4), 307-314.
30. Sari, A.; Alkan, C.; Kahraman Doguscu, D.; Bicer, A., Micro/nano-encapsulated n-heptadecane with polystyrene shell for latent heat thermal energy storage. *Sol. Energy Mater. Sol. Cells* **2014,** *126*, 42-50.
31. Sari, A.; Alkan, C.; Bicer, A.; Altuntas, A.; Bilgin, C., Micro/nanoencapsulated n-nonadecane with poly(methyl methacrylate) shell for thermal energy storage. *Energy Convers. Manage.* **2014,** *86*, 614-621.
32. Baek, K.-H.; Lee, J.-Y.; Kim, J.-H., Core/Shell Structured PCM Nanocapsules Obtained by Resin Fortified Emulsion Process. *J. Dispersion Sci. Technol.* **2007,** *28* (7), 1059-1065.
33. Alkan, C.; Sarı, A.; Karaipekli, A., Preparation, thermal properties and thermal reliability of microencapsulated n-eicosane as novel phase change material for thermal energy storage. *Energy Conversion and Management* **2011,** *52* (1), 687-692.
34. Zhang, G. H.; Bon, S. A. F.; Zhao, C. Y., Synthesis, characterization and thermal properties of novel nanoencapsulated phase change materials for thermal energy storage. *Sol. Energy* **2012,** *86* (5), 1149-1154.
35. Chen, Z. H.; Yu, F.; Zeng, X. R.; Zhang, Z. G., Preparation, characterization and thermal properties of nanocapsules containing phase change material n-dodecanol by miniemulsion polymerization with polymerizable emulsifier. *Applied Energy* **2012,** *91* (1), 7-12.
36. Fang, Y.; Yu, H.; Wan, W.; Gao, X.; Zhang, Z., Preparation and thermal performance of polystyrene/n-tetradecane composite nanoencapsulated cold energy storage phase change materials. *Energy Convers. Manage.* **2013,** *76*, 430-436.
37. Hu, X.; Huang, Z.; Zhang, Y., Preparation of CMC-modified melamine resin spherical nano-phase change energy storage materials. *Carbohydr. Polym.* **2014,** *101*, 83-88.
38. Nan, G.-h.; Wang, J.-p.; Wang, Y.; Wang, H.; Li, W.; Zhang, X.-x., Preparation and properties of nanoencapsulated phase change materials containing polyaniline. *Wuli Huaxue Xuebao* **2014,** *30* (2), 338-344.
39. Fang, G.; Li, H.; Yang, F.; Liu, X.; Wu, S., Preparation and characterization of nano-encapsulated n-tetradecane as phase change material for thermal energy storage. *Chem. Eng. J. (Amsterdam, Neth.)* **2009,** *153* (1-3), 217-221.

40. Latibari, S. T.; Mehrali, M.; Mehrali, M.; Afifi, A. B. M.; Mahlia, T. M. I.; Akhiani, A. R.; Metselaar, H. S. C., Facile synthesis and thermal performances of stearic acid/titania core/shell nanocapsules by sol–gel method. *Energy* **2015,** *85*, 635-644.
41. Latibari, S. T.; Mehrali, M.; Mehrali, M.; Mahlia, T. M. I.; Metselaar, H. S. C., Synthesis, characterization and thermal properties of nanoencapsulated phase change materials via sol–gel method. *Energy* **2013,** *61*, 664-672.
42. Zhu, Y.; Liang, S.; Chen, K.; Gao, X.; Chang, P.; Tian, C.; Wang, J.; Huang, Y., Preparation and properties of nanoencapsulated n-octadecane phase change material with organosilica shell for thermal energy storage. *Energy Conversion and Management* **2015,** *105*, 908-917.
43. Ho, K. M.; Li, W. Y.; Lee, C. H.; Yam, C. H.; Gilbert, R. G.; Li, P., Mechanistic study of the formation of amphiphilic core–shell particles by grafting methyl methacrylate from polyethylenimine through emulsion polymerization. *Polymer* **2010,** *51* (15), 3512-3519.
44. Hu, Y.; Jiang, X.; Ding, Y.; Ge, H.; Yuan, Y.; Yang, C., Synthesis and characterization of chitosan–poly(acrylic acid) nanoparticles. *Biomaterials* **2002,** *23* (15), 3193-3201.
45. Hopwood, D.; Allen, C. R.; McCabe, M., The reactions between glutaraldehyde and various proteins. An investigation of their kinetics. *The Histochemical Journal* **1970,** *2* (2), 137-150.
46. Jeong, S. G.; Jeon, J.; Lee, J. H.; Kim, S., Optimal preparation of PCM/diatomite composites for enhancing thermal properties. *International Journal of Heat and Mass Transfer* **2013,** *62*, 711-717.
47. Ford, T. J., Liquid-phase thermal decomposition of hexadecane: reaction mechanisms. *Industrial & Engineering Chemistry Fundamentals* **1986,** *25* (2), 240-243.
48. Jiang, K.; Su, Y.; Xie, B.; Jiang, S.; Zhao, Y.; Wang, D., Effect of Geometrical Confinement on the Nucleation and Crystallization Behavior of n-Alkane Mixtures. *The Journal of Physical Chemistry B* **2008,** *112* (51), 16485-16489.

Supporting Information

Nano-encapsulation Organic Phase Change Material in Water via Coacervation using Amphoteric Copolymer

Suqing Tan,[1] Albert P. C. Chan,[2] Pei Li*[1]

[1] Department of Applied Biology and Chemical Technology, The Hong Kong Polytechnic University, Hung Hom, Kowloon, Hong Kong, P. R. China

[2] Department of Building and Real Estate, The Hong Kong Polytechnic University, Hung Hom, Kowloon, Hong Kong, P. R. China

*Corresponding author: Email: pei.li@polyu.edu.hk

Figure S1. Morphology of the CTS-co-PMAA polymer observed with SEM image shows fiber-like structure.

Figure S2. CTS-co-PMAA at 80 °C (left) cooled to room temperature (right)

Figure S3. Turbidity of CTS-co-PMAA vs temperature, measured with 633 nm laser at 173°

Figure S4. Appearance of NEPCM dispersion in water and in dried powder.

Figure S5. Freezing curve of freeze dried NEPCMs and NEPCMs dried at room temperature

Figure S6. TGA curve of Chitosan (A) and CTS-co-PMAA (1:1) (B): 1) Degradation peak of CTS at 218 ^{0}C; 2) Degradation of the CTS-co-PMAA segment at 350℃; 3) Degradation of PMAA segment at 532 °C.

Figure S7. Particle size and size distribution of CTS-co-PMMA encapsulated hexadecane particles

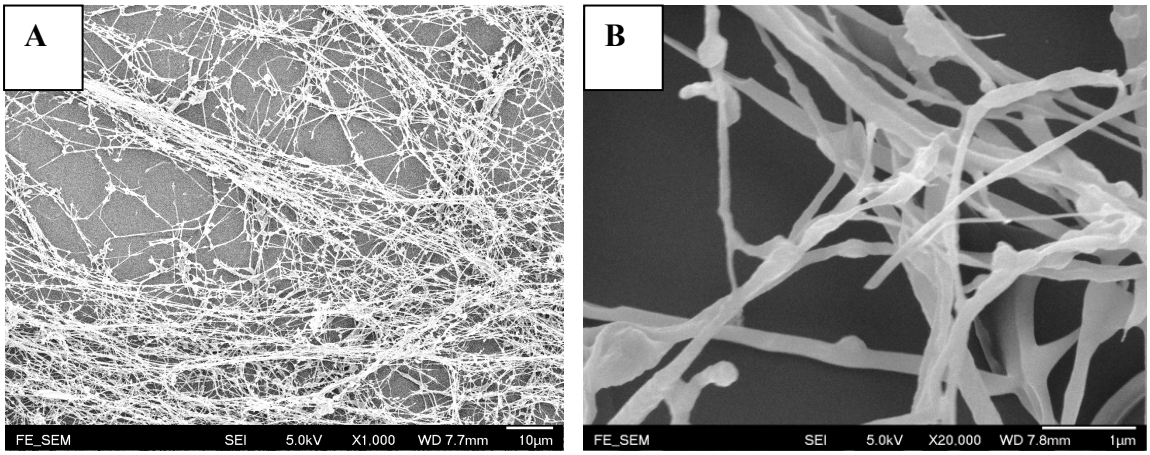

Figure S1. SEM image of CTS-co-PMAA (1:1 w/w) (Freeze dried) a) X1000; b) X20,000 magnification, showing fiber-like nanostructure.

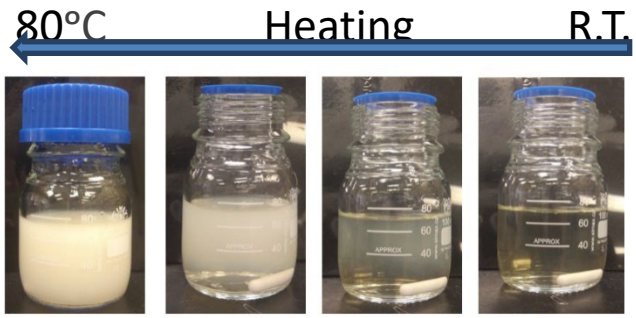

Figure S2. CTS-co-PMAA heated from room temperature (right) to 80 °C (left)

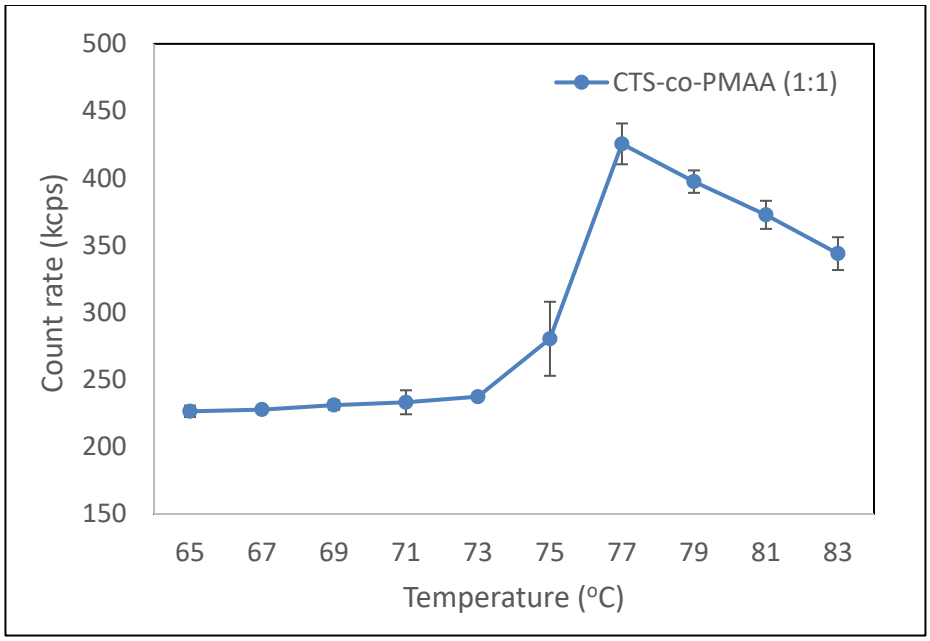

Figure S3. Turbidity of CTS-co-PMAA vs temperature, measured with 633 nm laser at 173°

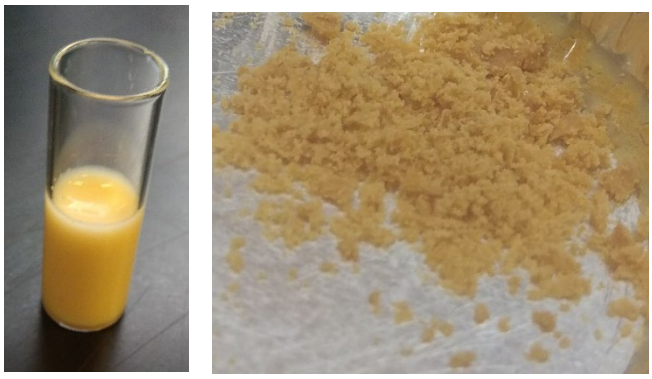

Figure S4. Appearance of NEPCM dispersion in water and in dried powder.

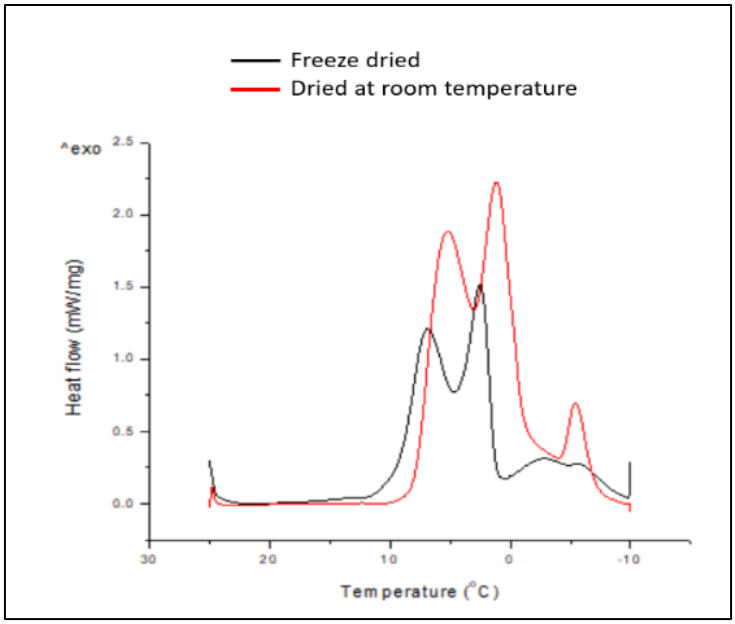

Sample	Freezing curve					%PCM
10EI16 RTF	LH_f (J/g)	T_{fo} (°C)	T_{fp} (°C)	T_{fe} (°C)	ΔT_f (°C)	
Freeze dried	105	11.7	2.5	0.7	-5.7	42%
		0.53	-2.7	-9.4		
Dried at room temperature	165	9.0	1.2	-7.9	-8.4	67%

Figure S5. Freezing curve of freeze dried NEPCMs and NEPCMs dried at room temperature

Thermal stability of chitosan and CTS-co-PMAA copolymer

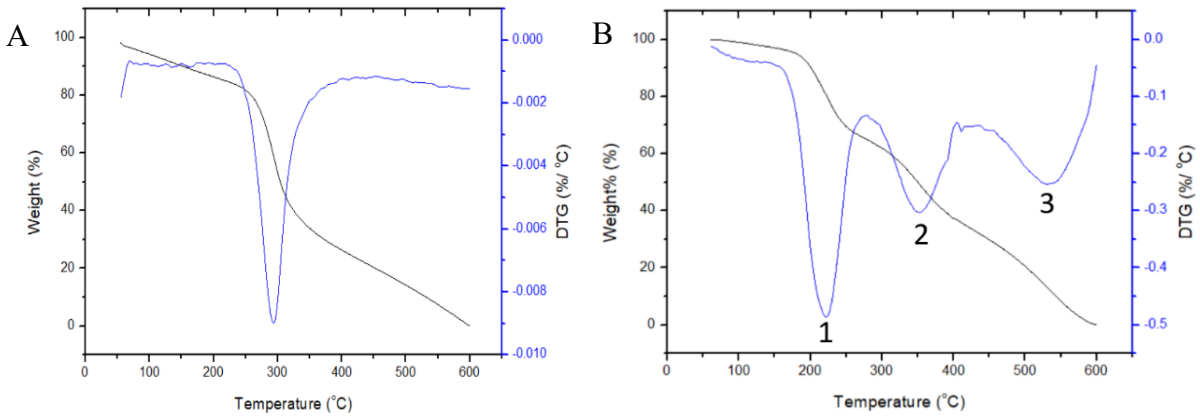

Figure S6. TGA curves of chitosan (A) and CTS-co-PMAA (1:1) (B): 1) Degradation peak of CTS at 218 ^{0}C; 2) Degradation of the CTS-co-PMAA segment at 350 ℃; 3) Degradation of PMAA segment at 532 ^{o}C.

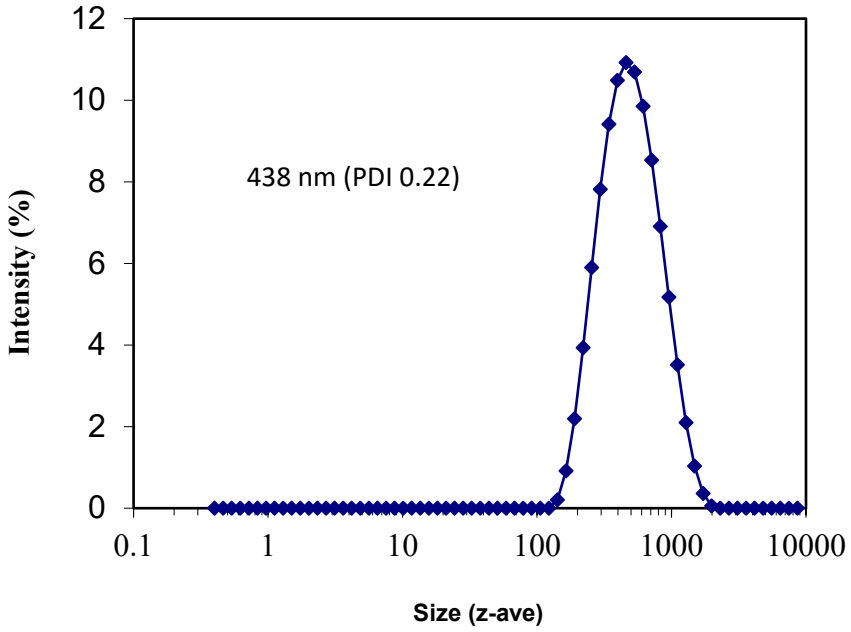

Figure S7. Particle size and size distribution of CTS-co-PMMA encapsulated hexadecane particles